

individual instances from the image itself, guiding the pretrained model to focus on the exclusive discriminative characteristics of the instances. To achieve this, we first design the image-level instance visual prompting to highlight the discriminative areas of instances in the input image, which comprises two complementary components of a patch prompt and a global prompt. By forwarding the input image to the designed lightweight prompters, the obtained patch prompt captures fine-grained local information from individual patches, meanwhile the global prompt gathers overall information from the entire image. Together, they complement each other in extracting the distinguishing regions of the instances, resulting in an instance image prompt that is overlaid onto the original image.

Furthermore, our InsVP also introduces the feature-level instance visual prompting to continuously incorporate instance information into the intermediate layers of the pretrained model. Considering both the commonalities and characteristics between different instances at the feature level, we design the learnable common prompt and the generated specific prompt respectively. Motivated by VPT [23], several learnable tokens are introduced as the common prompt to distill overarching patterns and fundamental attributes, fostering a comprehensive exploration of commonalities across all images. Moreover, a lightweight specific prompter is proposed to enhance the distinctive features specific to the individual instance from the input image itself. The collaboration between the common and specific prompts improves the adaptation capacity of the pretrained model to different instance samples, leading to superior performance. The main contributions of this work are:

- To address the limitations of existing visual prompting methods, we propose InsVP, an efficient approach aimed at comprehensively leveraging the discriminative instance-specific information of the input image itself to enhance the recognition capability of pretrained models.
- In InsVP, a novel image-level instance visual prompting scheme is designed to capture and emphasize the discriminative areas of different instances in the input image.
- Moreover, a complementary feature-level instance visual prompting model is developed in InsVP to direct the pretrained model to pay attention to the discriminative characteristics of the instances to facilitate feature extraction.
- Extensive experiments on various datasets show that our InsVP significantly outperforms the existing visual prompting methods with a much lower parameter cost.

2 RELATED WORK

2.1 Parameter-Efficient Finetuning

Vision Transformer (ViT) has made remarkable achievements in the field of computer vision [1, 7, 13, 30, 46]. However, with the rapid increase in model size, fully finetuning the pretrained ViT models for downstream tasks inevitably brings large storage and computing overhead. Therefore, recent works [16, 23, 53] started to focus on reducing the number of learnable parameters for efficient finetuning of pretrained models which can be broadly categorized into *partial tuning-based*, *extra module-based*, and *prompt learning-based* ones.

Partial tuning-based approaches [17, 35, 49, 54] aim to freeze the majority of the pretrained backbone while finetuning a small portion of the model parameters. For instance, such methods might only adjust the Linear/MLP heads [17, 21], or refine a part of layers within the backbone [35, 49, 54]. While these approaches are straightforward and simple to implement, they commonly exhibit a substantial performance gap when compared to fully finetuning [10, 32]. In contrast, extra module-based methods [5, 36, 38, 51, 53] design additional learnable plug-in architectures to finetune the pretrained model. [53] introduced an extra learnable side network while maintaining the original model frozen. Similarly, other studies [8, 36, 38] proposed to insert extra learnable residual units into the backbone. A limitation of these approaches lies in their customized nature for specific architectures, hindering generalizability to other models. Moreover, these modules obviously introduce more learnable parameters compared to partial tuning-based methods, making them difficult to apply in practice [16, 23].

2.2 Prompt Learning

Prompt learning techniques initially emerged in the field of natural language processing (NLP), involving the integration of a small set of learnable soft-prompt into input texts to tailor language models for specific downstream tasks [26–28]. Recent studies have extended prompt learning to visual tasks, termed visual prompt learning or visual prompting [3, 6, 16, 20, 23, 29, 48]. Compared with partial tuning-based and extra module-based methods, the visual prompting-based approaches introduce significantly fewer additional parameters and achieve better compatibility with models of different structures [16, 23].

Specifically, existing visual prompting methods usually follow two popular manners, task-level visual prompting [3, 16, 23, 41, 44, 48] and cluster-level visual prompting [20]. The former involves all downstream data samples learning a set of shared image prompts. VP [3] learned a single prompt for all samples, which is added around the image in the form of padding and then fed into the pretrained model together with the original image. VPT [23] introduced several learnable tokens as the prompt shared by all samples which are used in the multi-head self-attention (MSA) blocks of the pretrained ViT model. On the basis of VPT, E²VPT [16] pruned the learned prompts from both the token-wise and segment-wise perspectives, which reduces the impact of unfavorable prompts while reducing the number of additional parameters required. However, the above methods fail to capture the discriminative characteristics of instances, limiting the model performance [20]. The latest cluster-level visual prompting method DAM-VP [20] involved clustering samples and learning a set of visual prompts for each cluster. This approach partly mitigates the above problem, yet still struggles to capture subtle differences among instances within the same cluster. In addition, it will bring large parameter overhead, resulting in poor scalability. In contrast, our proposed InsVP introduces lightweight prompters to generate an instance prompt for each sample.

3 INSVP: INSTANCE VISUAL PROMPTING

In this section, we illustrate the proposed visual prompting method *InsVP* in detail. InsVP aims to generate instance-specific visual prompts for each individual image to adapt the pretrained model

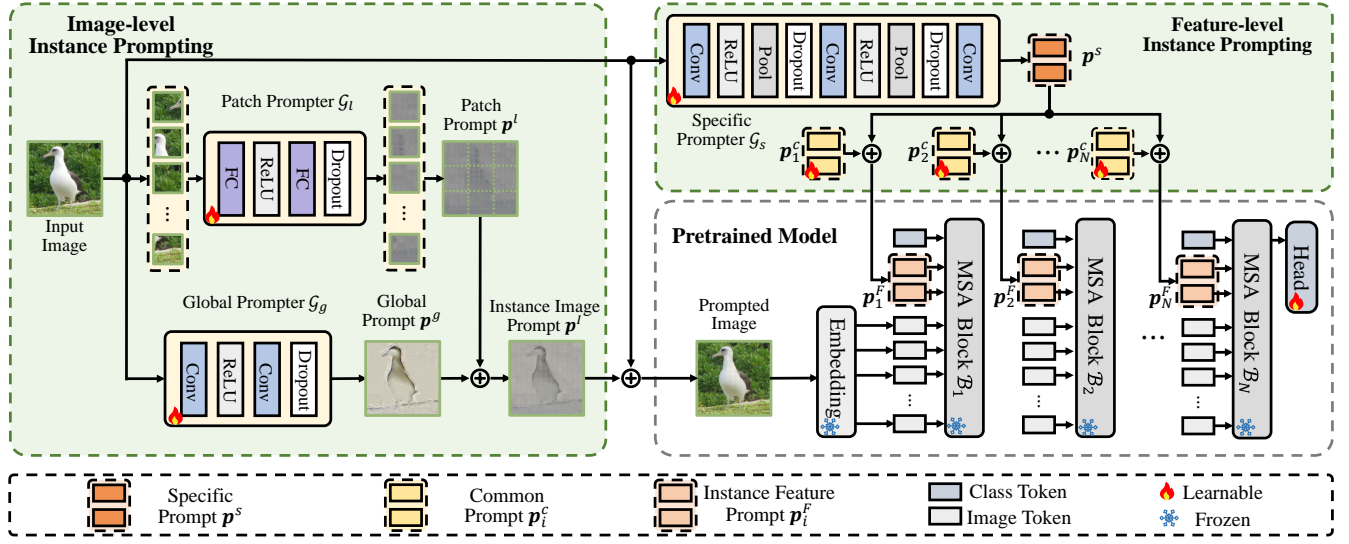


Figure 2: The pipeline of our proposed InsVP. For each image instance, InsVP first utilizes two lightweight prompters \mathcal{G}_l and \mathcal{G}_g to generate its patch prompt p^l and global prompt p^g respectively. Then they are merged into the instance image prompt p^I , which is further superimposed on the original image as the input of the pretrained model. Furthermore, the specific prompt \mathcal{G}_s is used to get the specific prompt p^s . It is merged with the learnable common prompt p_i^c to form the instance feature prompt p_i^F , which serves as the input tokens of the MSA blocks.

efficiently. The notations used in this paper are introduced in Section 3.1, followed by the introduction of the image-level instance prompting in Section 3.2 and feature-level instance prompting in Section 3.3. The overall pipeline of InsVP is depicted in Figure 2.

3.1 Preliminaries

For a pretrained Vision Transformer (ViT) [13] backbone \mathcal{M} , it contains N MSA blocks $\{\mathcal{B}_j\}_{j=1}^N$ where each \mathcal{B}_j consists of multi-head self-attention and feed-forward networks together with LayerNorm [2] and residual connections [18]. For an input image $\mathbf{x} \in \mathbb{R}^{H \times W \times C}$, it is initially divided into several equally sized patches $\{\mathbf{x}_i\}_{i=1}^M \in \mathbb{R}^{h \times w \times C}$, where (H, W) is the size of image \mathbf{x} , C is the number of channels of \mathbf{x} , (h, w) is the size of patch \mathbf{x}_i , M is the number of patches. Each patch \mathbf{x}_i is then first embedded into a d -dimensional latent space as:

$$\mathbf{h}_i^1 = \mathcal{E}(\mathbf{x}_i), \quad (1)$$

where $\mathbf{h}_i^1 \in \mathbb{R}^d$, $\mathcal{E}(\cdot)$ denotes the embedding layer of the backbone \mathcal{M} . Subsequently, all image tokens $\{\mathbf{h}_i^1\}_{i=1}^M$ along with an additional classification token $\mathbf{c}_1 \in \mathbb{R}^d$ are fed into the N MSA blocks $\{\mathcal{B}_j\}_{j=1}^N$ to extract features as:

$$\left[\mathbf{c}_{j+1}, \mathbf{h}_1^{j+1}, \dots, \mathbf{h}_M^{j+1} \right] = \mathcal{B}_j \left(\left[\mathbf{c}_j, \mathbf{h}_1^j, \dots, \mathbf{h}_M^j \right] \right), \quad (2)$$

where “[]” indicates stacking and concatenating on the sequence length dimension. Finally, the output \mathbf{c}_{N+1} from the last MSA block is passed through a classification head \mathcal{H} to derive the predicted probability distribution \mathbf{y} :

$$\mathbf{y} = \mathcal{H}(\mathbf{c}_{N+1}) \quad (3)$$

3.2 Image-level Instance Visual Prompting

To capture distinctive information of the input instance image \mathbf{x} , we initially propose image-level instance visual prompting, which involves generating the instance image prompt for each input image to improve the performance of the pretrained model \mathcal{M} .

Specifically, two lightweight networks, the global prompter \mathcal{G}_g and the patch prompter \mathcal{G}_l , are designed to readily explore the global and local discriminative characteristics of \mathbf{x} . The global prompter \mathcal{G}_g is composed of two layers of dilated convolution [50], along with a ReLU activation layer and a Dropout layer. The utilization of dilated convolution increases the receptive field of the global prompter \mathcal{G}_g without adding extra parameters, providing it with a broader global perspective across the entire image. Building on this design, the global prompter \mathcal{G}_g is capable of extracting global discriminative information from the original image \mathbf{x} via the generated prompt $\mathbf{p}^g \in \mathbb{R}^{H \times W \times C}$, such as the object’s position, shape, and contour details:

$$\mathbf{p}^g = \mathcal{G}_g(\mathbf{x}). \quad (4)$$

Additionally, to fully capture the locally fine-grained information of the individual image patch $\{\mathbf{x}_i\}_{i=1}^M$, a patch image prompter \mathcal{G}_l is leveraged. To generate the patch prompt efficiently, the patch prompter \mathcal{G}_l consists of two fully connected layers, taking a single image patch \mathbf{x}_i as input and producing the corresponding patch prompt p_i^l . This patch-based design significantly reduces the input and output dimensions of the fully connected layers, thereby decreasing the additional parameter overhead. By dividing the entire image \mathbf{x} into M patches $\{\mathbf{x}_i\}_{i=1}^M$, each patch \mathbf{x}_i is fed into the patch

prompter \mathcal{G}_l to obtain \mathbf{p}_i^l as below:

$$\mathbf{p}_i^l = \mathcal{G}_l(\mathbf{x}_i), \quad (5)$$

where $\mathbf{p}_i^l \in \mathbb{R}^{h \times w \times C}$. Subsequently, all $\{\mathbf{p}_i^l\}_{i=1}^M$ are concatenated in accordance with the relative order of the image patches $\{\mathbf{x}_i\}_{i=1}^M$, forming a complete patch prompt $\mathbf{p}^l \in \mathbb{R}^{H \times W \times C}$ for the input image \mathbf{x} .

Consequently, after generating the global image prompt \mathbf{p}^g and the patch prompt \mathbf{p}^l , the instance image prompt $\mathbf{p}^I \in \mathbb{R}^{H \times W \times C}$ for the input image \mathbf{x} is obtained by directly merging both two prompts in a linear combination manner to amalgamate the global and local information from the image itself:

$$\mathbf{p}^I = \beta_I \cdot \mathbf{p}^g + (1 - \beta_I) \cdot \mathbf{p}^l, \quad (6)$$

where β_I is a pre-defined weight hyper-parameter. Finally, the image prompt \mathbf{p}^I is superimposed onto the original image, serving as the input $\tilde{\mathbf{x}}$ of the pretrained model \mathcal{M} :

$$\tilde{\mathbf{x}} = \mathbf{x} + \mathbf{p}^I, \quad (7)$$

where $\tilde{\mathbf{x}} \in \mathbb{R}^{H \times W \times C}$ is the prompted image.

3.3 Feature-level Instance Visual Prompting

To further enhance the adaptation ability of the pretrained model \mathcal{M} , we design feature-level instance visual prompting to continuously incorporate instance-specific information into the MSA blocks. Given that at the feature level, different instances may exhibit both similarities and differences in their characteristics, our feature-level instance visual prompting proposes to utilize a common prompt \mathbf{p}^c and a specific prompt \mathbf{p}^s to simultaneously capture the commonality information among different instances and the distinctive information of each individual instance respectively.

Motivated by VPT [23], we introduce a number of L_p learnable tokens as the common prompt. For the sake of simplicity, we collectively denote all introduced tokens as \mathbf{p}^c without further distinction. The common prompt \mathbf{p}^c consists of distinct prompts added to each MSA block which is commonly used for all instances:

$$\mathbf{p}^c = \left\{ \mathbf{p}_j^c \right\}_{j=1}^N, \quad (8)$$

where $\mathbf{p}_j^c \in \mathbb{R}^{d \times L_p}$ is the common prompt for j -th MSA block \mathcal{B}_j .

As for the specific prompt $\mathbf{p}^s \in \mathbb{R}^{d \times L_p}$, it is directly obtained from the image \mathbf{x} itself. In detail, a three-layer convolutional network is designed as the specific prompter \mathcal{G}_s to generate \mathbf{p}^s for all MSA blocks:

$$\mathbf{p}^s = \mathcal{G}_s(\mathbf{x}). \quad (9)$$

Specifically, the specific prompter \mathcal{G}_s gradually employs convolutional and pooling layers to encode the image \mathbf{x} into $\mathbf{p}^s \in \mathbb{R}^{h \times w \times (C \cdot L_p)}$. Finally, the output \mathbf{p}^s is reshaped into the specific prompt $\mathbf{p}^s \in \mathbb{R}^{d \times L_p}$.

Subsequently, the complete instance feature prompt \mathbf{p}_j^F is formed by readily adding up the common prompt \mathbf{p}_j^c and specific prompt \mathbf{p}^s :

$$\mathbf{p}_j^F = \beta_F \cdot \mathbf{p}_j^c + (1 - \beta_F) \cdot \mathbf{p}^s, \quad (10)$$

where β_F is a pre-defined weight hyper-parameter. The instance feature prompt \mathbf{p}_j^F is combined with the image patch tokens $\{\mathbf{h}_i^j\}_{i=1}^M$

and the classification token \mathbf{c}_j , then collectively fed into the MSA block for feature extraction:

$$\left[\mathbf{c}_{j+1}, \hat{\mathbf{p}}_{j+1}^F, \mathbf{H}^{j+1} \right] = \mathcal{B}_j \left(\left[\mathbf{c}_j, \mathbf{p}_j^F, \mathbf{H}^j \right] \right), \quad (11)$$

where $\mathbf{H}^j = \left[\mathbf{h}_1^j, \mathbf{h}_2^j, \dots, \mathbf{h}_M^j \right]$. Notably $\hat{\mathbf{p}}_{j+1}^F$ get from \mathcal{B}_j is not utilized in the next block \mathcal{B}_{j+1} . Extensively extracting distinctive characteristics from images, the instance feature prompt \mathbf{p}^F and image prompt \mathbf{p}^I facilitate the pretrained model in capturing discriminative features of individual instances. Ultimately, the \mathbf{c}_{N+1} obtained from the final MSA block \mathcal{B}_N undergoes processing via a classification head \mathcal{H} to get the predicted probability distribution \mathbf{y} via Equation 3.

3.4 Overall Optimization

As mentioned above, our InsVP introduces only a few additional parameters:

$$\mathcal{G} = \{ \mathcal{G}_p, \mathcal{G}_g, \mathcal{G}_s, \mathbf{p}^c \}. \quad (12)$$

The extra parameters of InsVP are notably lightweight compared to the pretrained model and other visual prompting methods [16, 20, 23] as demonstrated in Section 4.4.5. Following previous works [16, 20, 23], during training, we maintain the pretrained model's encoder frozen while allowing only the classification head to be trainable. The optimization objective is as follows:

$$\arg \min_{\mathcal{G}, \mathcal{H}} \mathcal{L}_{ce}(\mathbf{y}, y_{gt}), \quad (13)$$

where \mathcal{L}_{ce} is cross-entropy loss, y_{gt} is the label of image \mathbf{x} .

4 EXPERIMENTS

4.1 Datasets

Building upon previous works [16, 20, 23], the experiments are conducted on four fine-grained datasets: CUB-200-2011 [43], NABirds [19], Oxford Flowers [34], and Stanford Dogs [24]. Additionally, following DAM-VP [20], we also perform experiments on another six commonly used visual datasets, including DTD [11], Food101 [4], Cifar100 [25], Cifar10 [25], GTSRB [40], and SVHN [33]. Following [23], for datasets with only publicly available train and test sets, we randomly split the train set into a train set (90%) and a validation set (10%), and utilize the validation set to determine hyper-parameters.

Additionally, we conduct experiments on the VTAB-1k benchmark [52] following [16, 23]. VTAB-1k is a benchmark that tests how well visual models perform across 19 different tasks. These tasks fall into three categories: Natural, for everyday image recognition; Specialized, for specific areas like medical images; and Structured, for understanding complex scenes, such as 3D object recognition.

4.2 Comparison Methods

We compare our InsVP with both parameter-efficient finetuning methods and visual prompting methods. We also report the fully-tuning results as a baseline. For parameter-efficient finetuning, we report the results of partial tuning-based methods including linear probing [21], Partial [49], MLP [17], and the results of extra module-based methods including Sidetune [38], Bias [53], Adapter [5],

Table 1: The comparison results against state-of-the-art methods on ten datasets. *Partial*, *Extra*, and *Prompting* represent partial tuning-based, extra module-based, and prompt learning-based parameter-efficient finetuning methods respectively. Following their paper, ILM-VP, Yoo et al and AutoVP utilize ResNeXt-101-32x8d [47], MoCo v3 trained ViT-B/16 and CLIP [37] as the backbone respectively. The best results are bolded and the second-best results are underlined.

Methods	Publication	DTD	CUB	Birds	Dogs	Flowers	Food	Cifar100	Cifar10	GTSRB	SVHN	Avg	
Full [21]	CVPR 2022	64.3	87.3	82.7	89.4	98.8	84.9	68.9	97.4	97.1	87.4	85.8	
<i>Partial</i>	Linear [21]	CVPR 2022	63.2	85.3	75.9	86.2	97.9	84.4	63.4	96.3	68.0	36.6	75.7
	Partial-1 [49]	NeurIPS 2014	70.1	85.6	77.8	85.5	98.2	83.8	78.0	95.0	89.3	82.4	84.6
	MLP-3 [9]	CVPR 2020	66.2	85.1	77.3	84.9	97.9	84.6	77.5	93.2	71.8	60.5	79.9
<i>Extra</i>	Bias [38]	NeurIPS 2017	69.8	88.4	84.2	91.2	98.8	86.2	82.9	96.9	89.9	82.5	87.1
	Sidetune [53]	ECCV 2020	57.7	84.7	75.8	85.8	96.9	78.7	68.8	90.4	90.9	80.5	81.0
	Adapter [5]	NeurIPS 2020	62.7	87.1	<u>84.3</u>	89.8	98.5	86.0	74.2	<u>97.7</u>	91.1	36.3	80.8
	AdaptFormer [8]	NeurIPS 2022	64.2	87.3	84.1	88.1	98.4	85.7	79.4	<u>96.5</u>	91.7	83.0	85.8
<i>Prompting</i>	VP [3]	arXiv 2022	59.5	84.6	77.7	84.5	97.7	80.5	78.7	94.2	89.4	87.6	83.4
	VPT [23]	CVPR 2022	65.8	<u>88.5</u>	84.2	90.2	<u>99.0</u>	83.3	78.8	96.8	90.7	78.1	85.5
	DAM-VP [20]	CVPR 2023	<u>73.1</u>	87.5	82.1	<u>92.3</u>	99.2	<u>86.9</u>	<u>88.1</u>	97.3	90.6	87.9	<u>88.5</u>
	ILM-VP [6]	CVPR 2023	41.4	7.7	11.6	87.6	27.9	23.0	45.9	81.7	59.9	81.4	46.8
	Yoo et al [48]	ICML 2023	69.6	82.9	76.0	83.4	93.7	82.9	85.8	97.3	92.6	90.1	85.4
	E ² VPT [16]	ICCV 2023	66.8	88.4	84.2	91.3	<u>99.0</u>	84.0	80.4	97.1	91.0	79.2	86.1
	TransHP [45]	NeurIPS 2023	68.4	87.1	82.7	91.5	98.6	85.5	86.9	97.3	91.3	82.9	87.2
	LION [44]	AAAI 2024	-	-	-	83.6	90.5	-	65.4	90.8	-	-	-
	AutoVP [41]	ICLR 2024	62.5	85.4	83.5	90.3	90.4	82.3	77.9	95.2	<u>93.1</u>	<u>92.9</u>	85.4
	InsVP(Ours)	This Paper	74.5	89.3	84.6	93.6	99.2	89.5	91.3	98.4	96.1	96.1	91.3

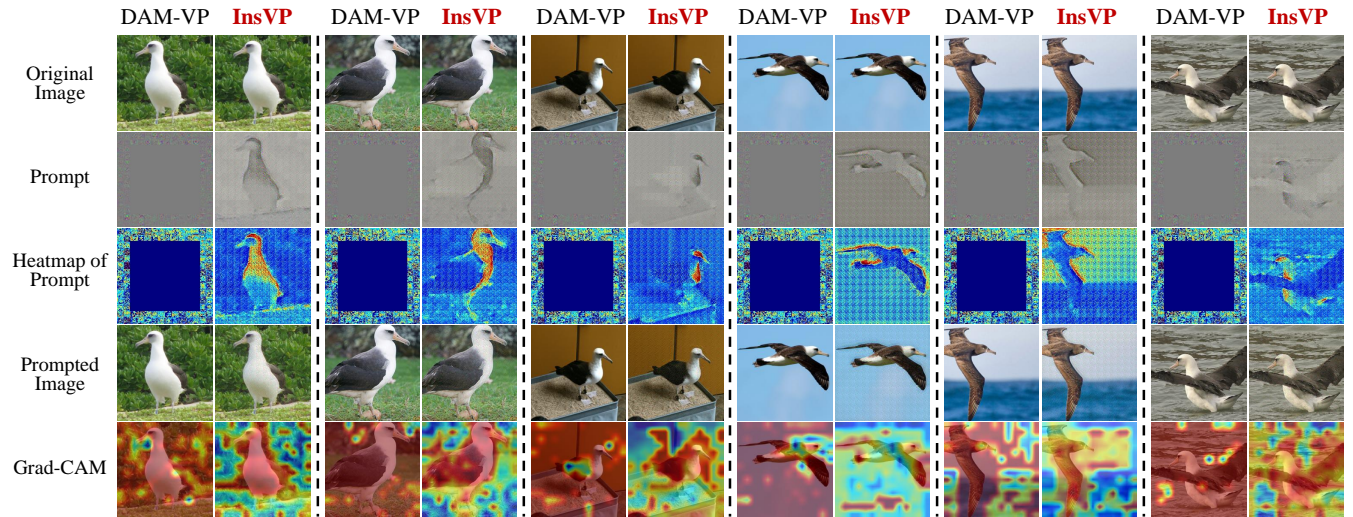


Figure 3: Visualization results of various instance samples in CUB. We present the original images along with the prompts of DAM-VP and our InsVP for the instances. Moreover, the heatmaps of the prompts, the prompted image, and the corresponding Grad-CAM visualization results are also presented.

AdaptFormer [8]. For visual prompting methods, we compare with the task-level visual prompting methods such as VP [3], VPT [23], ILM-VP [6], Yoo et al [48], E²VPT [16], LION [44], AutoVP [41] and the latest cluster-level visual prompting approach DAM-VP [20] and TransHP [45].

4.3 Implementation Details

Our experiments involve three pretrained vision models including the ViT-B/16 [13] and Swin Transformer [30] which are supervised

by ImageNet-21k [12], and another ViT-B/16 that is learned via MoCo v3 [10]. Following DAM-VP [20], we train for 100 epochs on all datasets. We utilize the AdamW [31] optimizer for optimization and implement cosine annealing. The hyper-parameters length of instance feature prompt L_p , fusion weight of image prompts β_I , and fusion weight of feature prompt β_F are set to 9, 0.7, and 0.5 respectively. The learning rate and weight decay on each dataset are detailed in the Supplementary Materials.

Table 2: The comparison results against state-of-the-art methods on VTAB-1k benchmark [52]. Following their paper, Yoo et al utilizes MoCo v3 trained ViT-B/16 as the backbone. Other methods utilize the ViT-B/16 [13] pretrained with supervised training on ImageNet-21k [12] as the backbone.

	Methods	VTAB-1k		
		Natural	Specialized	Structured
	Full [21]	75.9	83.4	47.6
<i>Partial</i>	Linear [21]	68.9	77.2	26.8
	Partial-1 [49]	69.4	78.5	34.2
	MLP-3 [9]	67.8	72.8	30.6
<i>Extra</i>	Bias [38]	73.3	78.3	44.1
	Sidetune [53]	58.2	68.1	23.4
	Adapter [5]	70.4	77.1	33.4
<i>Prompting</i>	VPT [23]	78.5	82.4	55.0
	Yoo et al [48]	74.8	83.4	49.1
	E ² VPT [16]	80.0	84.4	57.4
	InsVP(Ours)	81.8	85.2	58.4

Table 3: The comparison results of visual prompting methods on different network architectures. The Swin Transformer pretrained on ImageNet-21k is utilized as the backbone.

Methods	CUB	Birds	Cifar100	GTSRB	SVHN
Full [21]	89.7	86.8	73.3	97.1	91.2
VP [3]	86.5	82.9	80.6	82.4	80.3
VPT [23]	90.0	85.4	80.5	86.2	87.8
DAM-VP [20]	<u>90.4</u>	<u>86.9</u>	<u>88.1</u>	86.8	81.7
E ² VPT [16]	90.3	85.2	83.5	<u>87.1</u>	<u>88.2</u>
InsVP	91.2	87.7	90.3	90.1	91.4

Table 4: The comparison results of visual prompting methods on different pretraining methods. The MoCo-v3 learned ViT-B/16 is utilized as the backbone.

Methods	CUB	Birds	Cifar100	GTSRB	SVHN
Full [21]	78.8	72.8	84.0	96.8	90.6
VP [3]	75.4	69.0	79.1	89.8	<u>91.3</u>
VPT [23]	72.1	65.3	72.8	88.5	61.8
DAM-VP [20]	<u>79.7</u>	<u>71.4</u>	81.8	<u>92.8</u>	89.3
E ² VPT [16]	73.3	66.8	80.4	89.2	80.3
InsVP	80.2	72.8	83.5	95.6	92.7

4.4 Comparison with State-of-the-arts

4.4.1 Comparison on Pretrained ViT. We first conduct experiments on ten popular datasets using the ImageNet-21k supervised ViT-B/16 [13] as the pretrained model. As shown in Table 1, compared with other SOTA parameter-efficient finetuning and visual prompting methods, our InsVP exhibits a notable improvement of **3.5%** and **6.0%** on the GTSRB and SVHN respectively. Furthermore, across the other eight datasets, InsVP all achieves the best performance. Overall, compared with the second-best player, the cluster-level prompting method DAM-VP, our InsVP achieves an average improvement of 2.8% across the ten datasets. This is because our InsVP leverages image-level and feature-level instance visual prompting to elaborately capture discriminative characteristics of individual

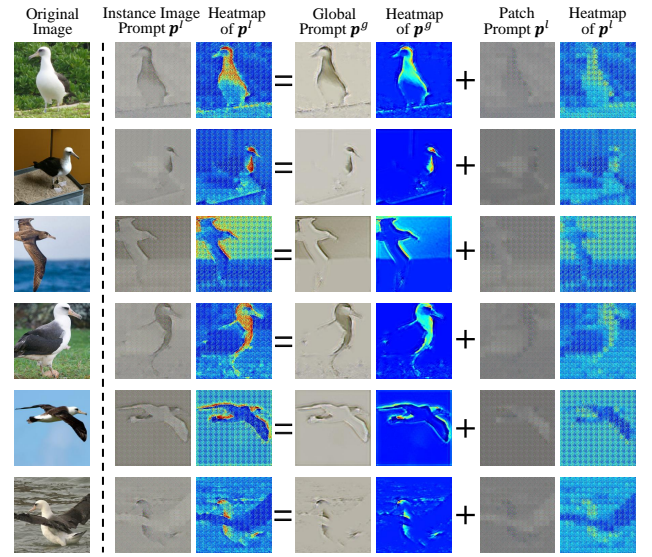


Figure 4: Visualization of the generated instance image prompt p^l , global prompt p^g , and patch prompt p^l through our InsVP method. The image prompt p^l is derived by adding the global prompt p^g and the patch prompt p^l together.

instances which enhance the pretrained model’s recognition capability, leading to more accurate prediction results.

To verify this, we further present the obtained prompts and Grad-CAM visualization results of the samples in CUB. As shown in Figure 3 and Figure 4, the visualization results reveal that DAM-VP employs the exact same prompt for the samples belonging to the same category but exhibiting significant differences. Moreover, it seems that the learned prompts of DAM-VP lack a direct connection with the image samples or categories, and explicit semantic information is not observed. The Grad-CAM visualization results also indicate that under their prompts, the pretrained model fails to focus on discriminative regions of the instances. In contrast, our InsVP precisely outlines the object and identifies discriminative regions, such as the location of the bird’s head and neck. Consequently, the pretrained model can more precisely focus on the object itself rather than the background, leading to outstanding performance.

4.4.2 Experiments on VTAB-1k Benchmark. To further validate the effectiveness of our InsVP, in addition to the ten datasets mentioned above, following [16, 23], we also conduct experiments on another widely used VTAB-1k [52] benchmark. As shown in Table 2, compared to the second-best method, E²VPT [16], InsVP achieve improvements of 1.8%, 0.8%, and 1.0% in the three different tasks *Natural*, *Specialized*, and *Structured*, respectively. This further illustrates the robust adaptability of our instance-level visual prompting designed based on the original image across diverse tasks.

4.4.3 Comparison on Different Model Architectures. To verify the generalization ability of our InsVP across different model architectures, we conduct experiments using the Swin Transformer [30] as the backbone. As shown in Table 3, although the Swin Transformer

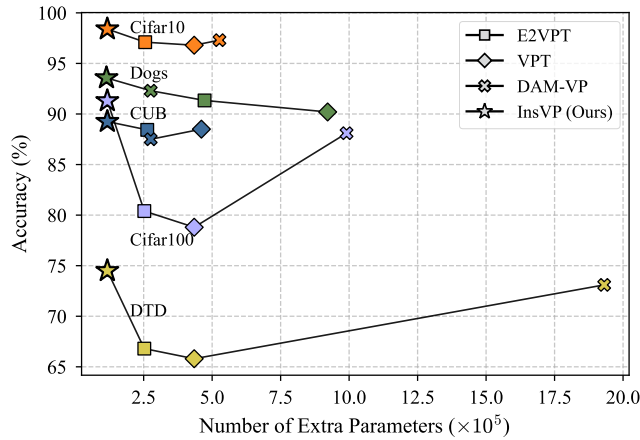


Figure 5: The comparison results of InsVP with other visual prompting methods in the number of extra parameters and model performance.

Table 5: Ablation study about the influence of components in InsVP. “-” and “✓” represent without or with this component. p^I represents the instance image prompt, comprising patch prompt p^I and global prompt p^g , and p^F represents the instance feature prompt, consisting of common prompt p^c and specific prompt p^s .

p^I		p^F		CUB	Birds	Cifar100	SVHN
p^I	p^g	p^c	p^s				
-	-	-	-	85.3	75.9	63.4	36.6
✓	-	-	-	87.1	83.1	85.5	85.3
✓	✓	-	-	87.9	83.5	87.0	91.8
✓	✓	✓	-	88.9	84.3	90.3	94.5
✓	✓	✓	✓	89.3	84.6	91.2	96.1

is a more advanced model that utilizes the shifted windows, compared with other visual prompting methods, our InsVP exhibits a consistent improvement of 1% to 3% across five datasets. This is because our InsVP is not designed for a specific network architecture. Instead, our InsVP directly extracts discriminative characteristics from each instance image itself, making it compatible with various pretrained model architectures.

4.4.4 *Comparison on Different Pretraining Methods.* In addition to supervised training, self-supervised contrastive learning, such as the MoCo paradigm [10], is also a commonly used method for model pretraining. To validate the generalization of our InsVP across different pretraining techniques, we conduct experiments based on the pretrained ViT-B/16 backbone via the MoCo v3 paradigm [10]. As reported in Table 4, our InsVP outperforms other visual prompting methods with an improvement ranging from 1% to 3% across five datasets consistently. This superiority is attributed to that our approach is directly tied to the characteristics of the data, showcasing enhanced adaptability to different pretraining paradigms compared to other methods.

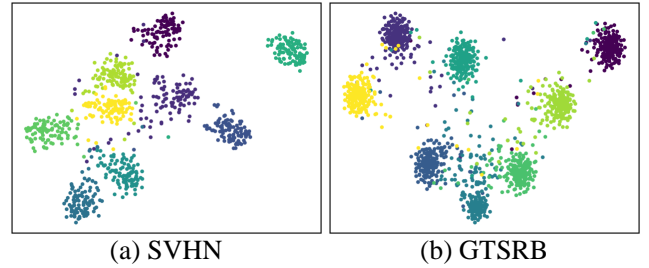


Figure 6: The t-SNE visualization results of specific prompt p^s generated by specific prompter G_s .

4.4.5 *Comparison of Extra Parameter Overhead.* For visual prompting methods, the number of introduced extra parameters is a crucial factor in determining their practical applicability. As illustrated in Figure 5, we compare the additional parameter quantities introduced by InsVP and other visual prompting methods. In the case of task-level visual prompting methods, since they use a shared prompt for all samples, a significant number of learnable tokens are required to capture diverse features of different samples. On the other hand, for cluster-level visual prompting methods like DAM-VP, a set of prompts needs to be learned for each cluster, resulting in a substantial increase of extra parameter overhead, reaching several times or even hundreds of times [20], thereby compromising the scalability.

In contrast, our proposed InsVP adopts a more straightforward methodology by extracting crucial prompting information directly from raw images. This allows InsVP to efficiently capture discriminative characteristics by lightweight prompters. Therefore, as shown in Figure 5, InsVP achieves optimal performance with minimal parameter costs.

4.5 Ablation

4.5.1 *Influence of Different Components.* To verify the effectiveness of different prompts in our proposed InsVP, ablation experiments are conducted on four datasets and reported in Table 5. As demonstrated, when neither component is used, the InsVP is degraded to a frozen pretrained ViT model with a learnable classifier. Taking results on CUB as an example, when using only the patch prompt p^I , the model’s performance improved by 1.8%. Furthermore, when both the patch prompt p^I and the global prompt p^g are used simultaneously, the model’s performance further increases by 0.8%. This is because the local information captured by the patch prompt p^I and the global information in the global prompt p^g can complement each other, allowing for more accurate extraction of discriminative information of individual instances. Moreover, when adding the feature-level common prompt p^c , it captures the common characteristics of all instances, resulting in an additional 1.0% improvement in model performance. Finally, with the addition of the generated specific feature prompt p^s , the complete InsVP is obtained. The specific prompt p^s extracts unique discriminative characteristics from individual instances, enabling the model to more accurately extract features for each instance and achieve the

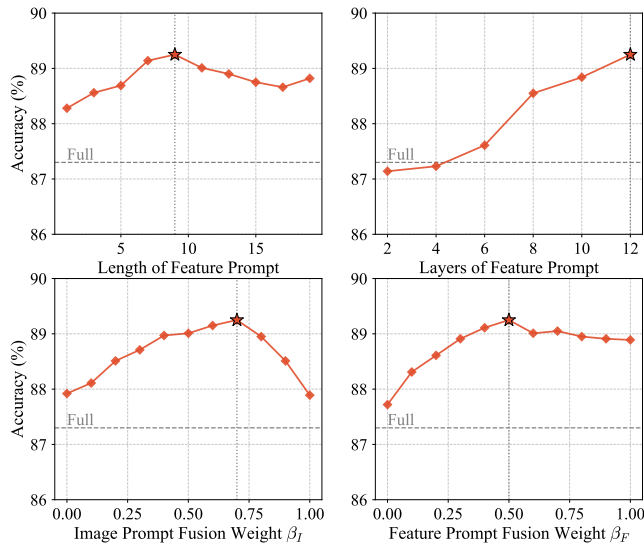


Figure 7: Influence of hyper-parameters of InsVP in CUB.

best performance. The results on other datasets also demonstrate a consistent trend to that observed on CUB.

4.5.2 *The t-SNE Visualization Results of Specific Prompt p^s* . To further explore the impact of the specific prompt, we perform t-SNE visualization for specific prompt p^s generated by specific prompter \mathcal{G}_s on SVHN and GTSRB datasets. As illustrated in Figure 6 below shows a notable correlation between specific prompts' distribution and sample categories. Despite being added to the middle layer of the network, specific prompts effectively capture discriminative information unique to individual instances, showing variability across different categories.

4.5.3 *Influence of Hyper-parameters*. The length of the feature prompt L_p and the number of MSA layers applied are two crucial hyper-parameters in our InsVP. To investigate their impact, we have conducted extensive ablation experiments. As depicted in Figure 7, the model's performance initially improves and then declines with the gradual increase of the feature prompt's length. This behavior arises due to the overfitting caused by an excessively large number of parameters with limited training data. Regarding the experiments on MSA layers, our feature prompt attains the best results when applied across all layers of ViT. This is because, at this point, the prompt can adapt the pretrained model across all network layers, enabling the pretrained model to better accommodate downstream tasks and consequently achieve superior performance.

We also conduct ablation experiments to assess the impact of image prompt fusion weight β_I and feature prompt fusion weight β_F . As depicted in Figure 7, when these two hyper-parameters are either too large or too small, the performance is degraded. When choosing intermediate values, patch prompt p^l , global prompt p^g , specific prompt p^s , and common prompt p^c can readily complement each other, fully unleashing the potential of our method.

4.5.4 *The t-SNE Visualization Results of Extracted Features*. As shown in Figure 8, we visualize the features obtained by InsVP and

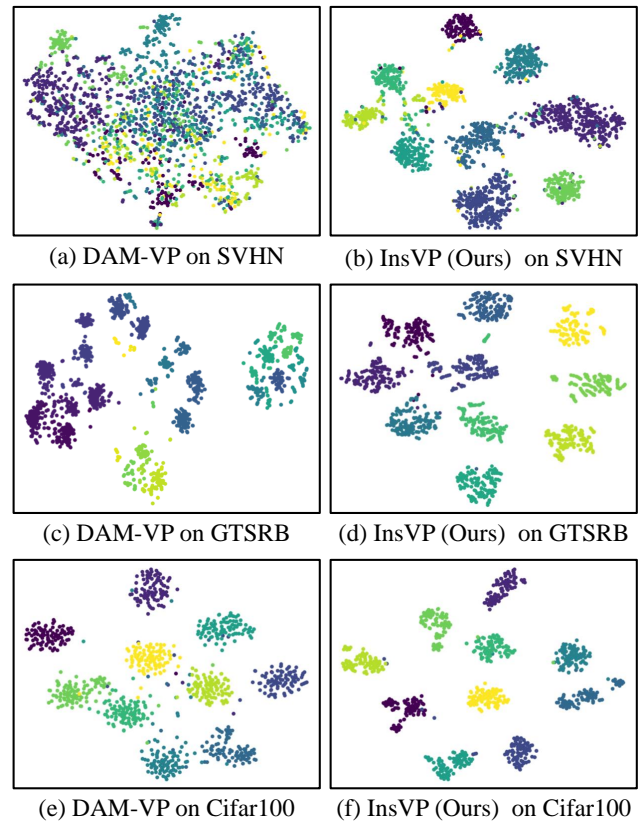


Figure 8: Feature t-SNE visualization results for InsVP and comparison method DAM-VP on three datasets.

DAM-VP via t-SNE [42]. From the visualization results, it is evident that the features extracted by DAM-VP from samples of the same category are relatively scattered, and some are mixed with features from other categories. In contrast, the features extracted by our InsVP from the same category are tightly clustered together, and they exhibit good distinctiveness from features of other categories. This is attributed to our instance image prompt and instance feature prompt, which can recognize the most essential discriminative characteristics of different category samples.

5 CONCLUSION

In this paper, we propose a novel and efficient instance visual prompting method, named InsVP. In comparison to the task-level or cluster-level visual prompting methods, our instance-level InsVP achieves outstanding performance by extracting discriminative characteristics of the individual instances using the proposed instance image prompt and instance feature prompt. We demonstrate that generating prompts directly from the original image itself is more efficient and the visualization results also illustrate our prompts are closely related to individual instances. In the future, it is interesting to further investigate how to explicitly explore hierarchical instance prompting to tackle instances with various recognition difficulties.

REFERENCES

- [1] Anurag Arnab, Mostafa Dehghani, Georg Heigold, Chen Sun, Mario Lučić, and Cordelia Schmid. 2021. ViViT: A Video Vision Transformer. In *2021 IEEE/CVF International Conference on Computer Vision (ICCV)*. 6816–6826. <https://doi.org/10.1109/ICCV48922.2021.00676>
- [2] Jimmy Lei Ba, Jamie Ryan Kiros, and Geoffrey E Hinton. 2016. Layer normalization. *arXiv preprint arXiv:1607.06450* (2016).
- [3] Hyojin Bahng, Ali Jahanian, Swami Sankaranarayanan, and Phillip Isola. 2022. Exploring visual prompts for adapting large-scale models. *arXiv preprint arXiv:2203.17274* (2022).
- [4] Lukas Bossard, Matthieu Guillaumin, and Luc Van Gool. 2014. Food-101—mining discriminative components with random forests. In *ECCV*. Springer International Publishing, Cham, 446–461.
- [5] Han Cai, Chuang Gan, Ligeng Zhu Massachusetts Institute of Technology, and Song Han Massachusetts Institute of Technology. 2020. TinyTL: reduce memory, not parameters for efficient on-device learning. In *Proceedings of the 34th International Conference on Neural Information Processing Systems* (, Vancouver, BC, Canada.) (NIPS '20). Curran Associates Inc., Red Hook, NY, USA, Article 947, 13 pages.
- [6] Aochuan Chen, Yuguang Yao, Pin-Yu Chen, Yihua Zhang, and Sijia Liu. 2023. Understanding and Improving Visual Prompting: A Label-Mapping Perspective. In *2023 IEEE/CVF Conference on Computer Vision and Pattern Recognition (CVPR)*. 19133–19143. <https://doi.org/10.1109/CVPR52729.2023.01834>
- [7] Chun-Fu Richard Chen, Quanfu Fan, and Rameswar Panda. 2021. CrossViT: Cross-Attention Multi-Scale Vision Transformer for Image Classification. In *2021 IEEE/CVF International Conference on Computer Vision (ICCV)*. 347–356. <https://doi.org/10.1109/ICCV48922.2021.00041>
- [8] Shoufa Chen, Chongjian Ge, Zhan Tong, Jiangliu Wang, Yibing Song, Jue Wang, and Ping Luo. 2022. Adapformer: Adapting vision transformers for scalable visual recognition. *Advances in Neural Information Processing Systems* 35 (2022), 16664–16678.
- [9] Xinlei Chen, Haoqi Fan, Ross Girshick, and Kaiming He. 2020. Improved baselines with momentum contrastive learning. *arXiv preprint arXiv:2003.04297* (2020).
- [10] Xinlei Chen, Saining Xie, and Kaiming He. 2021. An Empirical Study of Training Self-Supervised Vision Transformers. In *2021 IEEE/CVF International Conference on Computer Vision (ICCV)*. 9620–9629. <https://doi.org/10.1109/ICCV48922.2021.00950>
- [11] Mircea Cimpoi, Subhansu Maji, Iasonas Kokkinos, Sammy Mohamed, and Andrea Vedaldi. 2014. Describing Textures in the Wild. In *2014 IEEE Conference on Computer Vision and Pattern Recognition*. 3606–3613. <https://doi.org/10.1109/CVPR.2014.461>
- [12] Jia Deng, Wei Dong, Richard Socher, Li-Jia Li, Kai Li, and Li Fei-Fei. 2009. Imagenet: A large-scale hierarchical image database. In *CVPR*.
- [13] Alexey Dosovitskiy, Lucas Beyer, Alexander Kolesnikov, Dirk Weissenborn, Xiuhua Zhai, Thomas Unterthiner, Mostafa Dehghani, Matthias Minderer, Georg Heigold, Sylvain Gelly, et al. 2020. An image is worth 16x16 words: Transformers for image recognition at scale. *arXiv preprint arXiv:2010.11929* (2020).
- [14] Yunhui Guo, Yandong Li, Liqiang Wang, and Tajana Rosing. 2020. Adafilter: Adaptive filter fine-tuning for deep transfer learning. In *AAAI*.
- [15] Yunhui Guo, Honghui Shi, Abhishek Kumar, Kristen Grauman, Tajana Rosing, and Rogerio Feris. 2019. SpotTune: Transfer Learning Through Adaptive Fine-Tuning. In *2019 IEEE/CVF Conference on Computer Vision and Pattern Recognition (CVPR)*. 4800–4809. <https://doi.org/10.1109/CVPR.2019.00494>
- [16] Cheng Han, Qifan Wang, Yiming Cui, Zhiwen Cao, Wenguan Wang, Siyuan Qi, and Dongfang Liu. 2023. E²VPT: An Effective and Efficient Approach for Visual Prompt Tuning. *arXiv preprint arXiv:2307.13770* (2023).
- [17] Kaiming He, Haoqi Fan, Yuxin Wu, Saining Xie, and Ross Girshick. 2020. Momentum Contrast for Unsupervised Visual Representation Learning. In *2020 IEEE/CVF Conference on Computer Vision and Pattern Recognition (CVPR)*. 9726–9735. <https://doi.org/10.1109/CVPR42600.2020.00975>
- [18] Kaiming He, Xiangyu Zhang, Shaoqing Ren, and Jian Sun. 2016. Deep Residual Learning for Image Recognition. In *2016 IEEE Conference on Computer Vision and Pattern Recognition (CVPR)*. 770–778. <https://doi.org/10.1109/CVPR.2016.90>
- [19] Grant Van Horn, Steve Branson, Ryan Farrell, Scott Haber, Jessie Barry, Panos Ipeirotis, Pietro Perona, and Serge J. Belongie. 2015. Building a bird recognition app and large scale dataset with citizen scientists: The fine print in fine-grained dataset collection. In *CVPR*. IEEE Computer Society, 595–604.
- [20] Q. Huang, X. Dong, D. Chen, W. Zhang, F. Wang, G. Hua, and N. Yu. 2023. Diversity-Aware Meta Visual Prompting. In *2023 IEEE/CVF Conference on Computer Vision and Pattern Recognition (CVPR)*. 10878–10887.
- [21] Eugenia Iofinova, Alexandra Peste, Mark Kurtz, and Dan Alistarh. 2022. How Well Do Sparse ImageNet Models Transfer?. In *2022 IEEE/CVF Conference on Computer Vision and Pattern Recognition (CVPR)*. 12256–12266. <https://doi.org/10.1109/CVPR52688.2022.01195>
- [22] Yunhun Jang, Hankook Lee, Sung Ju Hwang, and Jinwoo Shin. 2019. Learning what and where to transfer. In *ICML*. PMLR.
- [23] Menglin Jia, Luming Tang, Bor-Chun Chen, Claire Cardie, Serge Belongie, Bharath Hariharan, and Ser-Nam Lim. 2022. Visual prompt tuning. In *Computer Vision – ECCV 2022*. Springer Nature Switzerland, Cham, 709–727.
- [24] Aditya Khosla, Nityananda Jayadevaprakash, Bangpeng Yao, and Fei-Fei Li. 2011. Novel dataset for fine-grained image categorization: Stanford dogs. In *CVPRW*.
- [25] Alex Krizhevsky, Geoffrey Hinton, et al. 2009. Learning multiple layers of features from tiny images. (2009).
- [26] Brian Lester, Rami Al-Rfou, and Noah Constant. 2021. The power of scale for parameter-efficient prompt tuning. *arXiv preprint arXiv:2104.08691* (2021).
- [27] Xiang Lisa Li and Percy Liang. 2021. Prefix-tuning: Optimizing continuous prompts for generation. *arXiv preprint arXiv:2101.00190* (2021).
- [28] Xiao Liu, Kaixuan Ji, Yicheng Fu, Weng Lam Tam, Zhengxiao Du, Zhilin Yang, and Jie Tang. 2021. P-tuning v2: Prompt tuning can be comparable to fine-tuning universally across scales and tasks. *arXiv preprint arXiv:2110.07602* (2021).
- [29] Yajing Liu, Yuning Lu, Hao Liu, Yaozu An, Zhuoran Xu, Zhuokun Yao, Baofeng Zhang, Zhiwei Xiong, and Chenguang Gui. 2023. Hierarchical Prompt Learning for Multi-Task Learning. In *2023 IEEE/CVF Conference on Computer Vision and Pattern Recognition (CVPR)*. 10888–10898. <https://doi.org/10.1109/CVPR52729.2023.01048>
- [30] Z. Liu, Y. Lin, Y. Cao, H. Hu, Y. Wei, Z. Zhang, S. Lin, and B. Guo. 2021. Swin Transformer: Hierarchical Vision Transformer using Shifted Windows. In *2021 IEEE/CVF International Conference on Computer Vision (ICCV)*. IEEE Computer Society, Los Alamitos, CA, USA, 9992–10002. <https://doi.org/10.1109/ICCV48922.2021.00986>
- [31] Ilya Loshchilov and Frank Hutter. 2017. Decoupled weight decay regularization. *arXiv preprint arXiv:1711.05101* (2017).
- [32] Dhruv Mahajan, Ross Girshick, Vignesh Ramanathan, Kaiming He, Manohar Paluri, Yixuan Li, Ashwin Bharambe, and Laurens Van Der Maaten. 2018. Exploring the limits of weakly supervised pretraining. In *Computer Vision – ECCV 2018*. Springer International Publishing, Cham, 185–201.
- [33] Yuval Netzer, Tao Wang, Adam Coates, Alessandro Bissacco, Bo Wu, and Andrew Y Ng. 2011. Reading digits in natural images with unsupervised feature learning. (2011).
- [34] Maria-Elena Nilsback and Andrew Zisserman. 2008. Automated Flower Classification over a Large Number of Classes. In *2008 Sixth Indian Conference on Computer Vision, Graphics and Image Processing*. 722–729. <https://doi.org/10.1109/ICVGIP.2008.47>
- [35] Mehdi Noroozi and Paolo Favaro. 2016. Unsupervised learning of visual representations by solving jigsaw puzzles. In *Computer Vision – ECCV 2016*. Springer International Publishing, Cham, 69–84.
- [36] Jonas Pfeiffer, Andreas Rücklé, Clifton Poth, Aishwarya Kamath, Ivan Vulić, Sebastian Ruder, Kyunghyun Cho, and Iryna Gurevych. 2020. Adapterhub: A framework for adapting transformers. *arXiv preprint arXiv:2007.07779* (01 2020), 46–54. <https://doi.org/10.18653/v1/2020.emnlp-demos.7>
- [37] Alec Radford, Jong Wook Kim, Chris Hallacy, Aditya Ramesh, Gabriel Goh, Sandhini Agarwal, Girish Sastry, Amanda Askell, Pamela Mishkin, Jack Clark, et al. 2021. Learning transferable visual models from natural language supervision. In *ICML*. PMLR.
- [38] Sylvestre-Alvise Rebuffi, Hakan Bilen, and Andrea Vedaldi. 2017. Learning multiple visual domains with residual adapters. In *Proceedings of the 31st International Conference on Neural Information Processing Systems* (Long Beach, California, USA) (NIPS'17). Curran Associates Inc., Red Hook, NY, USA, 506–516.
- [39] Ramprasaath R. Selvaraju, Michael Cogswell, Abhishek Das, Ramakrishna Vedantam, Devi Parikh, and Dhruv Batra. 2017. Grad-CAM: Visual Explanations from Deep Networks via Gradient-Based Localization. In *2017 IEEE International Conference on Computer Vision (ICCV)*. 618–626. <https://doi.org/10.1109/ICCV.2017.74>
- [40] Johannes Stallkamp, Marc Schlipsing, Jan Salmen, and Christian Igel. 2012. Man vs. computer: Benchmarking machine learning algorithms for traffic sign recognition. *Neural networks* 32 (2012), 323–332. <https://doi.org/10.1016/j.neunet.2012.02.016>
- [41] Hsi-Ai Tsao, Lei Hsiung, Pin-Yu Chen, Sijia Liu, and Tsung-Yi Ho. 2024. AutoVP: An Automated Visual Prompting Framework and Benchmark. In *The Twelfth International Conference on Learning Representations*.
- [42] Laurens Van der Maaten and Geoffrey Hinton. 2008. Visualizing data using t-SNE. *Journal of machine learning research* (2008).
- [43] Catherine Walch, Steve Branson, Peter Welinder, Pietro Perona, and Serge Belongie. 2011. The caltech-ucsd birds-200-2011 dataset. (2011).
- [44] Haixin Wang, Jianlong Chang, Xiao Luo, Jinan Sun, Zhouchen Lin, and Qi Tian. 2023. Lion: Implicit vision prompt tuning. *arXiv preprint arXiv:2303.09992* (2023).
- [45] Wenhao Wang, Yifan Sun, Wei Li, and Yi Yang. 2024. Transhp: Image classification with hierarchical prompting. *Advances in Neural Information Processing Systems* 36 (2024).
- [46] Wenhao Wang, Enze Xie, Xiang Li, Deng-Ping Fan, Kaitao Song, Ding Liang, Tong Lu, Ping Luo, and Ling Shao. 2021. Pyramid Vision Transformer: A Versatile Backbone for Dense Prediction without Convolutions. In *2021 IEEE/CVF International Conference on Computer Vision (ICCV)*. 548–558. <https://doi.org/10.1109/ICCV48922.2021.00061>
- [47] Saining Xie, Ross Girshick, Piotr Dollár, Zhuowen Tu, and Kaiming He. 2017. Aggregated Residual Transformations for Deep Neural Networks. In *2017 IEEE*

929
930
931
932
933
934
935
936
937
938
939
940
941
942
943
944
945
946
947
948
949
950
951
952
953
954
955
956
957
958
959
960
961
962
963
964
965
966
967
968
969
970
971
972
973
974
975
976
977
978
979
980
981
982
983
984
985
986987
988
989
990
991
992
993
994
995
996
997
998
999
1000
1001
1002
1003
1004
1005
1006
1007
1008
1009
1010
1011
1012
1013
1014
1015
1016
1017
1018
1019
1020
1021
1022
1023
1024
1025
1026
1027
1028
1029
1030
1031
1032
1033
1034
1035
1036
1037
1038
1039
1040
1041
1042
1043
1044

1045	<i>Conference on Computer Vision and Pattern Recognition (CVPR)</i> . 5987–5995. https://doi.org/10.1109/CVPR.2017.634	
1046	[48] Seungryong Yoo, Eunji Kim, Dahuin Jung, Jungbeom Lee, and Sungroh Yoon. 2023. Improving Visual Prompt Tuning for Self-supervised Vision Transformers. <i>arXiv preprint arXiv:2306.05067</i> (2023).	
1047	[49] Jason Yosinski, Jeff Clune, Yoshua Bengio, and Hod Lipson. 2014. How transferable are features in deep neural networks?. In <i>Proceedings of the 27th International Conference on Neural Information Processing Systems - Volume 2 (Montreal, Canada) (NIPS'14)</i> . MIT Press, Cambridge, MA, USA, 3320–3328.	
1048	[50] Fisher Yu, Vladlen Koltun, and Thomas Funkhouser. 2017. Dilated Residual Networks. In <i>2017 IEEE Conference on Computer Vision and Pattern Recognition (CVPR)</i> . 636–644. https://doi.org/10.1109/CVPR.2017.75	
1049	[51] Elad Ben Zaken, Shauli Ravfogel, and Yoav Goldberg. 2021. Bitfit: Simple parameter-efficient fine-tuning for transformer-based masked language-models. <i>arXiv preprint arXiv:2106.10199</i> (2021).	1103
1050	[52] Xiaohua Zhai, Joan Puigcerver, Alexander Kolesnikov, Pierre Ruyssen, Carlos Riquelme, Mario Lucic, Josip Djolonga, Andre Susano Pinto, Maxim Neumann, Alexey Dosovitskiy, et al. 2019. A large-scale study of representation learning with the visual task adaptation benchmark. <i>arXiv preprint arXiv:1910.04867</i> (2019).	1104
1051	[53] Jeffrey O Zhang, Alexander Sax, Amir Zamir, Leonidas Guibas, and Jitendra Malik. 2020. Side-Tuning: A Baseline for Network Adaptation via Additive Side Networks. In <i>Computer Vision – ECCV 2020</i> . Springer International Publishing, Cham, 698–714.	1105
1052	[54] Richard Zhang, Phillip Isola, and Alexei A Efros. 2016. Colorful image colorization. In <i>Computer Vision – ECCV 2016</i> . Springer International Publishing, Cham, 649–666.	1106
1053		1107
1054		1108
1055		1109
1056		1110
1057		1111
1058		1112
1059		1113
1060		1114
1061		1115
1062		1116
1063		1117
1064		1118
1065		1119
1066		1120
1067		1121
1068		1122
1069		1123
1070		1124
1071		1125
1072		1126
1073		1127
1074		1128
1075		1129
1076		1130
1077		1131
1078		1132
1079		1133
1080		1134
1081		1135
1082		1136
1083		1137
1084		1138
1085		1139
1086		1140
1087		1141
1088		1142
1089		1143
1090		1144
1091		1145
1092		1146
1093		1147
1094		1148
1095		1149
1096		1150
1097		1151
1098		1152
1099		1153
1100		1154
1101		1155
1102		1156